JACS
JOURNAL OF THE AMERICAN CHEMICAL SOCIETY
Article
pubs.acs.org/JACS

Brute-Force Hyperpolarization for NMR and MRI

Matthew L. Hirsch,[†] Neal Kalechofsky,*[,‡] Avrum Belzer,[‡] Melanie Rosay,[†] and James G. Kempf*[,†]

[†]Bruker Biospin Corp., Billerica, Massachusetts 01821, United States
[‡]Millikelvin Technologies, LLC, Braintree, Massachusetts 02184, United States

Supporting Information

ABSTRACT: Hyperpolarization (HP) of nuclear spins is critical for ultrasensitive nuclear magnetic resonance (NMR) and magnetic resonance imaging (MRI). We demonstrate an approach for >1500-fold enhancement of key small-molecule metabolites: 1-^{13}C-pyruvic acid, 1-^{13}C-sodium lactate, and 1-^{13}C-acetic acid. The ^{13}C solution NMR signal of pyruvic acid was enhanced 1600-fold at B = 1 T and 40 °C by pre-polarizing at 14 T and ∼2.3 K. This "brute-force" approach uses only field and temperature to generate HP. The noted 1 T observation field is appropriate for benchtop NMR and near the typical 1.5 T of MRI, whereas high-field observation scales enhancement as 1/B. Our brute-force process ejects the frozen, solid sample from the low-T, high-B polarizer, passing it through low field (B < 100 G) to facilitate "thermal mixing". That equilibrates ^{1}H and ^{13}C in hundreds of milliseconds, providing ^{13}C HP from ^{1}H Boltzmann polarization attained at high B/T. The ejected sample arrives at a room-temperature, permanent magnet array, where rapid dissolution with 40 °C water yields HP solute. Transfer to a 1 T NMR system yields ^{13}C signals with enhancements at 80% of ideal for noted polarizing conditions. High-resolution NMR of the same product at 9.4 T had consistent enhancement plus resolution of ^{13}C shifts and J-couplings for pyruvic acid and its hydrate. Comparable HP was achieved with frozen aqueous lactate, plus notable enhancement of acetic acid, demonstrating broader applicability for small-molecule NMR and metabolic MRI. Brute-force avoids co-solvated free-radicals and microwaves that are essential to competing methods. Here, unadulterated samples obviate concerns about downstream purity and also exhibit slow solid-state spin relaxation, favorable for transporting HP samples.

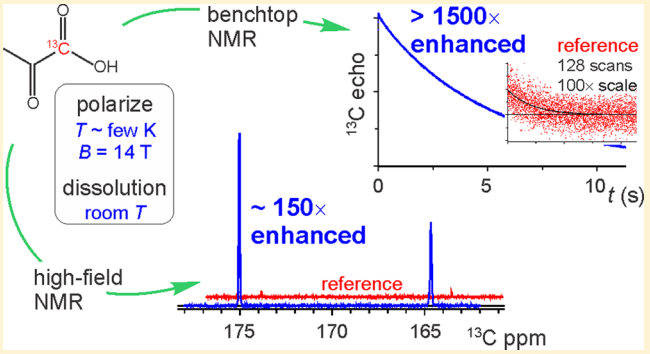

INTRODUCTION

There is broad interest and prominent recent development in hyperpolarization (HP) of nuclear spins. By dramatically increasing signal intensities, HP can greatly extend the analytical reach of nuclear magnetic resonance (NMR) and open new areas of magnetic resonance imaging (MRI) for medical diagnosis and for evaluation of therapeutic efficacy. This huge potential is best underscored by the most general of current HP techniques: dynamic nuclear polarization (DNP), as applied in both solids NMR[1,2] and its solids-into-liquids counterpart, dissolution DNP (d-DNP).[3] Solids DNP offers up to several-hundred-fold sensitivity gains, enabling high-resolution NMR of challenging biomolecules,[4] surfaces,[5] and pharmaceutical formulations.[6] Meanwhile, d-DNP can enhance sensitivity more than 10 000-fold in solution-state measurements near room temperature. That opens the door to an array of new applications, including measurement of the real-time kinetics of enzymes[7−9] via HP substrates and living polymers[10] via HP monomers, drug discovery from assays of HP ligands,[11,12] studies of cell metabolism,[13] biomolecular characterization using HP water,[14] and ultrafast collection of multi-dimensional spectra for applications to mass-limited samples.[15]

In MRI, hyperpolarization enables imaging of dilute compounds and nuclei with a low gyromagnetic ratio (γ). For example, ^{13}C-enriched metabolites provide background-free detection and sufficient spin lifetimes to be tracked during circulation and uptake. This has been possible only via gains from HP by d-DNP or other, more chemically specific approaches, such as those based on chemical transfers of HP from parahydrogen.[16−21] The most prominent imaging applications of d-DNP are for cancer screening. This has enabled MRI-tracked uptake and conversion of HP ^{13}C-labeled metabolites,[22] for example, revealing the telltale elevation of pyruvate-to-lactate conversion in breast cancer[23] and lymphoma.[24] Most significantly, the first human diagnostic MRI study with HP ^{13}C-pyruvate recently succeeding in identifying prostate cancer in 31 of 31 patients tested.[25] This included identifying cancerous regions missed by standard methods.

In spite of these successes, the alternative method of "brute-force" HP offers several advantages over d-DNP, parahydrogen, and other[26−29] strategies. Brute-force utilizes just two factors to hyperpolarize a molecule: low temperature (T) and high magnetic field (B). As in d-DNP, brute-force HP is targeted to

Received: February 4, 2015
Published: June 22, 2015

DOI: 10.1021/jacs.5b01252
J. Am. Chem. Soc. 2015, 137, 8428−8434

NMR or MRI experiments following *dissolution* of the sample at near room temperature. Unlike d-DNP, no free-radicals, microwave excitation, or co-solvents are needed. Two obvious advantages result. First, radicals are unwanted contaminants, so their absence avoids the need for downstream filtering and quality assurance. Second, brute-force may be more general, relying only on Boltzmann-law polarization rather than secondary chemistry or physics. These advantages are similar to those over parahydrogen techniques, which utilize catalytic metals for chemical transformation of,[16] or transient association with,[19] the molecular targets of HP.

A further advantage is that the extraction of samples pre-polarized by brute force is unhampered by radical-induced spin relaxation, a particular concern in the solid state and/or at the low fields traversed when removing a sample for measurement. Manageable relaxation in radical-free samples can enable *transport* of HP molecules held at modest B and T. For example, we found that frozen 1-^{13}C-pyruvic acid near 50 K and 2 T has a longitudinal relaxation time $T_1(^{13}C)$ of ∼1 h, and ∼24 h if dropping to 10 K. Thus, it could be delivered to imaging facilities as a HP agent, avoiding barriers to use such as cost of and expertise with the polarizing apparatus. Widespread precedent for similar off-site production exists in positron emission tomography (PET) using 2-deoxy-2-(^{18}F)fluoro-D-glucose (1.8 h half-life).[30]

Finally, the absence of microwaves expands the scalability of production by avoiding sample confinement to an excitation cavity. Ultimately, this may be a key to overcoming the main drawback of brute force: waiting. Although long T_1 values favor transport, values exceeding 100 h in sub-kelvin regimes can prohibit high-throughput production. Parallel production of multiple samples can combat that and is workable with our method. High-B, but low-homogeneity, large-bore (here, 103 mm) magnets can accommodate many samples cooled in a single cryostat. [See also the Supporting Information (SI) discussion on cryogenic considerations for multi-sample cooling in the mK regime.]

Here we demonstrate our approach to brute-force polarization, followed by solid-state extraction and conversion to solution-state HP. Warming the sample while in the solid state presents unique challenges. Key unknowns to overcome here include (a) crossing the minimum of T_1 vs T, known as the "valley of death", where polarization obtained under cryogenic conditions rapidly dissipates, and (b) transferring ^{1}H→^{13}C polarization by "thermal mixing" as the ejected, warming sample traverses fields down to 0.02 T in ∼1 s. Remarkably, the combined steps succeeded with at most 20% loss of the polarization produced in the cryostat. This is in spite of the fact that relaxation in the noted T_1 valley occurs on a time scale <1 s for temperatures 75−150 K, even for fields 100-fold larger than that experienced during thermal mixing.

The overall process we used is shown schematically in Figure 1a, where the caption describes steps for low-T polarization, ejection combined with ^{1}H →^{13}C polarization transfer (low-field thermal mixing, LFTM), and finally dissolution for NMR observation. Each step following polarization increases the sample temperature, and so we overlay the steps on a plot of the thermal equilibrium values of ^{1}H and ^{13}C spin polarizations vs T. Without HP, room-temperature samples exhibit just ppm advantages of spin-up vs spin-down populations. This is due to tiny energy differences between these states (42.6 and 10.7 MHz/T for ^{1}H and ^{13}C). Brute-force HP combats this problem by making ultra-low-temperature (ULT), high-field polarization

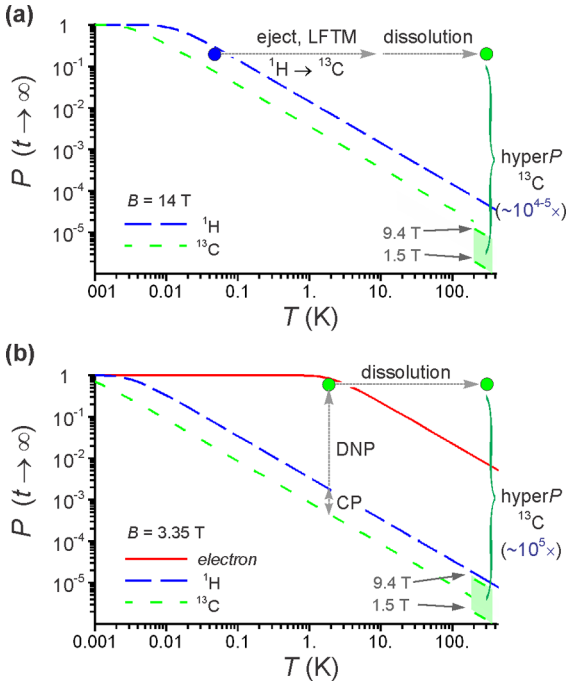

Figure 1. Polarization curves and schemes for solids-to-liquids hyperpolarization (HP). (a) Brute-force HP, with polarization (P) vs T for ^{1}H and ^{13}C in a 14 T pre-polarizing field. The overlaid process depicts ultralow temperature (ULT) polarization of protons and then ejection of the cold, solid sample through conditions (B < ∼100G) for low-field thermal mixing, which equilibrates ^{13}C spins with the pre-polarized protons. Next is dissolution and then measurement of ^{13}C HP in a detection field from the shaded range (green), pertinent to MRI (1.5, 3 T), or from benchtop to high-resolution NMR (1−9.4 T). (b) Dissolution DNP, similarly depicted, at its typical 3.35 T. ^{13}C polarization may be achieved by direct DNP from electron−^{13}C coupling, or by ^{1}H DNP plus CP to ^{13}C to significantly reduce buildup times.[32,33]

levels available for observation at the warm temperatures and range of fields typical to solution NMR (shaded green region in Figure 1a). This covers from 1.5 T in conventional MRI to about 9.4 T, representative of fields for solution NMR. Further, the low-field end, down to 1 T, is relevant for benchtop NMR, which is an increasingly valuable tool for chemical analysis.[31]

The benefits of pre-polarizing at much lower T (and higher B) are obvious from the plot. For example, samples near 100 mK and at 14 T have natural equilibrium polarizations 4−5 orders of magnitude higher than at the B and T values targeted for NMR observation. Even relatively modest cryogenics (1−4 K) can enhance sensitivity by factors of 10^3−10^4. As shown in Figure 1b, d-DNP yields such gains at more modest T. But that requires a vertical connection to highly polarized radical electron spins using resonant microwaves (i.e., DNP), possibly in concert with ^{1}H−^{13}C cross-polarization (CP).[32,33] Brute-force incorporates neither the gains nor the drawbacks of those methods, yet it offers noted advantages of scalable sample production and the potential for transportable HP.

■ RESULTS AND DISCUSSION

Sensitivity gains >1500× at 1 T, relevant to imaging or benchtop NMR, and ∼150× for 9.4 T, high-resolution NMR were obtained by the process summarized in Figure 1a. Systems and methods used are detailed in the Experimental Section. In brief, frozen samples were held at cryogenic T and B = 14 T for

DOI: 10.1021/jacs.5b01252
J. Am. Chem. Soc. 2015, 137, 8428−8434

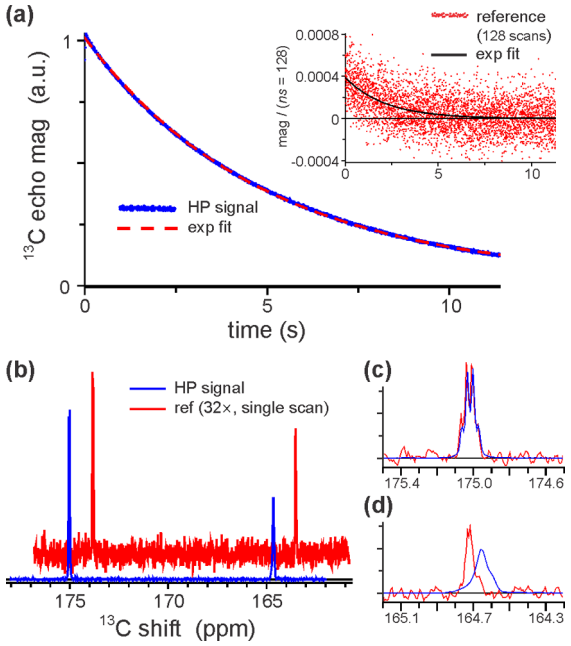

Figure 2. Brute-force HP ^{13}C NMR from 1-^{13}C-pyruvic acid. (a) ^{13}C echo train at B_0 = 1 T and 40 °C from the dissolution product of a sample polarized at 2.1−2.5 K and 14 T. Inset: signal-averaged reference from the same sample, equilibrated to 1 T, 40 °C using 128 scans at 200 s recycle delay. (b) High-resolution ^{13}C spectrum at 9.4 T from a separate aliquot of the same dissolution product. (c,d) Zoom to peaks of pyruvic acid and pyruvate hydrate near 175 and 165 ppm, respectively.

a period of pre-polarization. Next, pneumatic ejection removed samples to a room-temperature station for dissolution into warm water. ^{13}C NMR proceeded after the solution was transferred to a 1 T or 9.4 T NMR system. Gains on the latter are ∼10× lower than at 1 T.

Results from neat 1-^{13}C-pyruvic acid, pre-polarized near 2.3 K and 14 T, are shown in Figure 2a. The HP ^{13}C signal at B_0 = 1 T was measured within 3 s of dissolution. It is an echo-decay profile, where each point i is the integration of a 0.25 ms echo window in a train from the sequence $(\pi/2)_x-[\tau-(\pi)_y-\tau]_n$, with τ = 1.5 ms, t_π = 40 μs, and n = 3800. The HP "magnitude signal" (explicitly defined in the Experimental Section) is a factor ε = (1630 ± 180) times larger than the average result from four single-shot reference signals collected at intervals of 5 min (∼5 × T_1). This corresponds to a polarization, $P(^{13}C)$ = 0.13%, that is 80% of the ideal achievable had ^{13}C fully equilibrated to pre-polarization conditions. A signal-averaged reference (Figure 2a, inset) was also collected over the subsequent 8 h. Its initial echo intensity is 2500× that of the HP signal. Larger apparent enhancements were typical from signal-averaged vs single-shot references. However, that is likely due to destructive interference of co-added scans, and we prefer the conservative result from averaging several single-shot references.

The apparent losses (∼20%) are incurred during (a) the several 100 ms ejection, including passage through low-field (20 G minimum), (b) a subsequent 2−3 s of ambient warming in the 2 T dissolution station, and (c) the final solution-state transit through Earth's field on the way to measurement. The latter appears to account for the majority, i.e., 15% loss (see SI Figure 1), and might be lessened by transfer in a modest field[34] (>100 G) and/or by adding an O_2 scavenger to the dissolution water.[35] Finally, another pair of results indicates that losses before ejection are insignificant. Both were obtained from pre-polarization at 1.9 K and 14 T, for ε = (610 ± 40) and (690 ± 40). The slightly larger value came despite tripling of the 50 s typically experienced at $T \approx$ 10−12 K in preparation for ejection. Thus, re-equilibration is negligible during a T rise of that scale and duration.

We also detailed chemically resolved enhancements for the aqueous equilibrium between pyruvic acid and pyruvate hydrate. Figure 2b is a high-resolution ^{13}C spectrum (9.4 T, 100 MHz ^{13}C frequency) collected from an aliquot split-off at dissolution of the same sample that gave the 1 T result of Figure 2a. The aliquot for high-resolution NMR arrived 20 s after dissolution. Accounting for the added ∼17 s decay in transit (SI Figure 1), the ratio of integrated HP and reference spectra yielded high-field enhancement consistent with that at 1 T.

At the pyruvic acid peak (∼165 ppm, Figure 2d), enhancements were reproducibly 15−18% larger than from pyruvate hydrate (∼175 ppm, Figure 2c). The HP peak from pyruvic acid is also shifted and broadened relative to its reference peak (single-shot spectrum, collected 5 min after the HP result). This reproducible distinction may be due to incomplete mixing and equilibration prior to collection of the HP signal. The hydrate shows no such change and may be less susceptible to inhomogeneities, e.g., of T, pH, viscosity, etc. Origins of the noted differential enhancement are less clear, as the two species appear to have matching relaxation during the Earth's-field transit to the NMR magnet. [For example, see SI Figure 1, but note, it reports relaxation measured on an equilibrated sample.]

Polarization for ∼10 h appears sufficient to achieve these enhancements, although T_1 data are not yet available for exact quantitation. Results in Figure 2 followed much longer polarization (70 h near 2.3 K). However, in a separate run, just 13 h near 3.0 K yielded similar ε = (1170 ± 70) for ^{13}C at 1 T. That corresponds to $P(^{13}C)$ = 0.10%, which again is 80% of ideal for polarizing conditions.

Finally, a similar approach with sodium 1-^{13}C-lactate (aqueous, 20% w/w) yielded $\varepsilon \approx$ 500−700× from ∼2.7 K for 4 h in one instance and ∼20 h in another. These correspond to $P(^{13}C) \approx$ 0.05%, or ∼40% of ideal from these conditions. We also succeeded in our single attempt with 1-^{13}C-acetic acid (2.6 K for 17 h), but obtained only $\varepsilon \approx$ 60×, for $P(^{13}C)$ = 0.005%, or ∼4% of ideal. [HP and reference signals for lactate and acetic acid are provided in SI Figure 2.]

These results demonstrate potential broader applicability of brute-force HP. However, further study is required to define whether conditions should be tailored for better performance by mitigating unique losses on ejection and/or in the solution state. For example, we observed aqueous 1-^{13}C-acetic acid and sodium 1-^{13}C-lactate with twice the loss rate at B = 5 G that aqueous 1-^{13}C-pyruvic acid exhibits. That loss might be avoided by maintaining ∼500 G during transfer between dissolution and NMR steps.[34] In addition, losses on ejection may differ from those of pyruvic acid due to distinctly located T_1 minima vs T ranging 4−200 K. The minima are set by the freedom of methyl rotations, which are known to vary vs physical preparation of the sample[36] and thus expected to vary somewhat vs molecular structure.

The efficiency of ^{13}C buildup in our approach leverages the relatively rapid development of ^{1}H polarization (e.g., $T_1(^1H) \approx 0.1 \times T_1(^{13}C)$ for polarizing conditions of Figure 2).

DOI: 10.1021/jacs.5b01252
J. Am. Chem. Soc. 2015, 137, 8428−8434

Equilibration into ^{13}C occurs subsequently in the process known as low-field thermal mixing (LFTM).[37,38] Pneumatic sample ejection through a region with $B < \sim 100$ G activates LFTM as the field drops to a threshold where ^{1}H and ^{13}C are in spectral overlap. The cutoff is set by the local, dipolar field, which dominates their line widths. LFTM brings heteronuclei to a common "spin temperature" determined by the level of pre-polarization in each spin I_i and their "spin specific heats",

$$C_i = p_i I_i(I_i + 1)(\gamma_i)^2 \quad (1)$$

where p_i is the fractional sample content of spin I_i with gyromagnetic ratio γ_i. Neat, 99%-enriched 1-^{13}C-pyruvic acid has normalized C_i values for ^{1}H at methyl and carboxylic sites of 0.738 and 0.246, compared to a remarkably small 0.016 for ^{13}C (in spite of full isotopic enrichment at C_1). Dominant ^{1}H specific heats mean that LFTM establishes essentially the full ^{1}H pre-polarization level on *both* nuclei. [See also discussion in the SI.] This buildup of $P(^{13}C)$ with retention of $P(^{1}H)$ can be an advantage over more-familiar transfer schemes, such as CP. LFTM also avoids confinement to an NMR coil, which simplifies scalability to multiple samples. A second advantage is that $P(^{1}H)$ can be sourced either intermolecularly, as from methyls in neat pyruvic acid, or from protic solvents, e.g., water in our HP of 1-^{13}C-lactate. A disadvantage is that LFTM does not add enhancement by γ_H/γ_X as in CP. Rather, LFTM yields no more polarization on the low-γ nucleus than could have been achieved by waiting out direct equilibration to pre-polarizing conditions.

Though LFTM has been understood for over 50 years,[37,38] recently other groups have also recognized its value for HP transfer.[39−41] There, LFTM was performed on stationary samples by cycling from a high polarizing field to near zero for mixing, and then back up for NMR detection. Tens of minutes are typically needed for such field cycling, whereas our ejection process requires <1 s and is a natural fit with solid-state extraction of brute-force HP.

Finally, we explored potential for further brute-force gains, including the possibility of reaching enhancements on par with d-DNP. That entails pre-polarization in sub-Kelvin regimes, where continued $1/T$ scaling is expected down to ~30 mK for ^{1}H at 14 T (to ~10 mK for ^{13}C). The main challenge is a T_1-imposed waiting time, and, when polarizing near 500 mK, we obtained only modest returns. Using 24 h pre-polarization, these dissolution products exhibited no more than $\varepsilon \approx 600$ at 1 T [$P(^{13}C) = 0.05\%$]. Figure 3 plots output vs polarizing T to reveal fading ε_{24h} below ~2 K for 1-^{13}C-pyruvic acid. Loss profiles on ejection are independent of the polarizing T, so this must be attributed to slower pre-polarization. In other words, as T drops in the 0.5−3 K regime, $T_1(^{1}H)$ grows more quickly than the equilibrium polarization, whose profile follows $P = \tanh(\gamma_H B_0/2k_B T) \propto (1/T)$, as in Figure 1a.

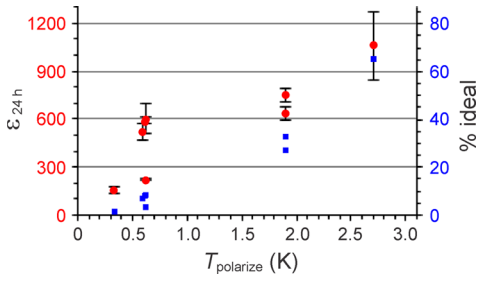

Figure 3. ^{13}C enhancements vs pre-polarization T in 1-^{13}C-pyruvic acid, as observed by pre-polarizing for $t_{pol} \approx 24$ h, and scaled to that common time assuming P was in its linear phase of growth ($t_{pol} \ll T_1$). The trend to reduced efficiency in attaining ε as T drops is especially clear when representing the same data as percent of the ideal ε achievable (blue squares) at the given polarizing T.

In spite of the excellent 2−4 K performance, Figure 3 reveals a remaining challenge for brute-force HP. We have proven the most efficient approach to achieve low-γ HP without resorting to irradiation or spin relaxation agents. The latter are ideally avoided both for potential loss contributions during extraction and as unwanted contaminants. Another point against relaxation agents is that they would diminish the time available for storage/transport of HP samples. Instead, the challenge of long polarization times can be tackled by re-engineering to accommodate multi-sample production.

Nonetheless, increasing absolute throughput may be desirable in spite of the trade-offs of relaxation agents. In key recent work, Gadian, Owers-Bradley, and co-workers reduced T_1 by ~10× for ^{1}H and ^{13}C in frozen aqueous 1-^{13}C-sodium acetate admixed with chelated lanthanides. There, Dy- and Ho-based agents were effective down to 1 K.[39,42] Better results followed with Cu nanoparticles, giving >100-fold drops across temperatures ranging 20 mK to ~1 K.[43] Because such agents can be quantitatively filtered and exhibit limited effects on solution relaxation, they are promising for combination with the methods presented here. Other approaches, such as application of mere monolayers of ^{3}He, to reduce T_1 of nuclei in a high surface-to-volume sample, also offer increased throughput. For example, Friedman et al. discovered a 10-fold drop in ^{19}F T_1 for fluoropolymers in low-T, high-B conditions,[44] while Owers-Bradley found a similar effect from ^{3}He as a relaxation switch when polarizing ^{129}Xe near 200 mK.[45] With ^{3}He, removal is straightforward, even prior to sample ejection.

CONCLUSIONS

Brute-force polarization, solid-state extraction, and conversion to solution-state HP offer a new approach for the fields of NMR and MRI. We reached 10^3-fold gains at a field relevant to both MRI and emerging benchtop solution NMR applications, as well as 10^2-fold gains for high-resolution NMR. Furthermore, this was achieved with the lone molecule of demonstrated diagnostic value in HP imaging.[25]

A key milestone here is our crossing of the T_1 "valley of death" with no more than 20% loss, and simultaneously passing ^{1}H polarization onto ^{13}C by low-field thermal mixing. The generality and simplicity of low-T, high-B polarization combined with LFTM and dissolution provides several advantages to complement dissolution DNP. Critically, extracting brute-force polarization in the solid state opens the door for transport of HP on slowly relaxing low-γ nuclei. For example, in a 2 T field achievable from permanent magnets, $T_1(^{13}C)$ is nearly 1 h at 50 K and up to 24 h near 10 K in 1-^{13}C-pyruvic acid. For context, this is 10 times longer than the ^{18}F half-life utilized for transport in PET imaging.

Although the best enhancements from d-DNP remain much larger (~100×), these initial brute-force results are already sufficient for many applications. For example, ^{13}C imaging in animals at ~8 μL voxel size (well within the preferred range of 1−27 μL) is possible even at 1 T. Imaging at 3 or 7 T can push to 1 μL voxels, while polarization of larger samples could enable

DOI: 10.1021/jacs.5b01252
J. Am. Chem. Soc. 2015, 137, 8428−8434

human imaging. These estimates assume a doubling of HP losses en route to the sample (e.g., an *in vivo* tumor) and a 5 mM concentration of 1-^{13}C-pyruvic acid at the imaged site. For ^{13}C NMR, >1000-fold gains are immediately noteworthy as 10 times the value available from isotopic enrichment. In combination with multi-sample handling (to reduce the per-sample throughput), this could enable new applications in mixture/component analysis and evaluation of sample-limited compounds (e.g., in natural products synthesis). The promise of HP is also widely acknowledged across surface science, medicinal chemistry, in-cell metabolism, and chemical or biomolecular structure, dynamics, and kinetics.[46,47] Here, it can be delivered at moderate cost relative to d-DNP, without the challenges and limitations of co-added radicals and microwaves, and with far greater generality than current parahydrogen or optical methods.

Our brute-force approach should also be extensible beyond present small molecules, in which motions of methyl groups establish time scales of polarization buildup and loss. Proteins and a variety of polymer chains are loaded with methyls, and similar ^{1}H,^{13}C results are thus expected. Meanwhile, other chemical functionality may likewise facilitate efficient brute-force HP (e.g., ^{13}C-, ^{15}N-, or ^{31}P-bearing groups containing or vicinal to protons). As with other HP methods, the main challenge for biomolecules will likely be in combining complex multi-dimensional NMR with the "single-shot utility" of HP. Nonetheless, that problem can be overcome by encoding different time steps for multi-dimensional NMR in distinct spatial regions of the solution NMR sample.[48]

EXPERIMENTAL SECTION

The Polarizer. The polarization environment was controlled using a Kelvinox 400 (Oxford Instruments) dilution refrigerator (DR) with a magnet operating up to 14 T. The apparatus to handle sample insertion, polarization, and ejection is shown in Figure 4a. This "U-tube" insert to the DR was built to our design by ICE Oxford Ltd. It consists of one arm connected to our gas-handling system (GHS), with 99.999% He source (^{4}He only). As shown in the inset to Figure 4a, the sample and a "wad" (to assist pneumatic ejection) rest on a cross wire just on the other side of the U-turn, in the adjoined insert/eject (I/E) arm. Calibrated Cernox sensors (Lakeshore Cryotronics) were placed at several locations, including on heat exchangers at ∼125 K and ∼6 K and on the exterior of oxygen-free, high-thermal-conductivity (OFHC) Cu segments at the U-tube base.

On the I/E arm, T ranges from 5 to 10 K over ∼90% of its 1.8 m length, as measured during light flow (2.7 L/min of He at 3 bar) with a sensor held in the path. Cooling the I/E arm is key to mitigating polarization losses on ejection. We achieved it via a series of 3-in.-long copper clasps soldered to the exterior of the stainless-steel I/E arm. Clasps reside between pairs of baffles along the helical upper section and are joined by OFHC braids. This arrangement is ultimately coupled to the DR's 4 K plate (not shown), which is even with the 6 K heat exchanger depicted in Figure 4a.

Sample Preparation. Samples were prepared in a N_2 drybox by injecting ∼40 μL of neat, deoxygenated 1-^{13}C-pyruvic acid (Cambridge Isotope Laboratories) into a mold with a Teflon-coated pin to push the sample onto the interior wall of a polycarbonate shuttle (Figure 4b). Samples were frozen over a period of hours by placing the mold into a −30 °C (243 K) freezer integrated to the drybox. After being extracted from the mold, samples were removed from the drybox for further handling or direct loading to the polarizer using a "magazine" at −30 °C. This insulated the sample from room temperature and provided airtight fittings to admit the sample to the polarizer without air exposure.

Sample Introduction. Samples were introduced to the U-tube under slight positive pressure (2.7 L/min flow). First, a Teflon wad

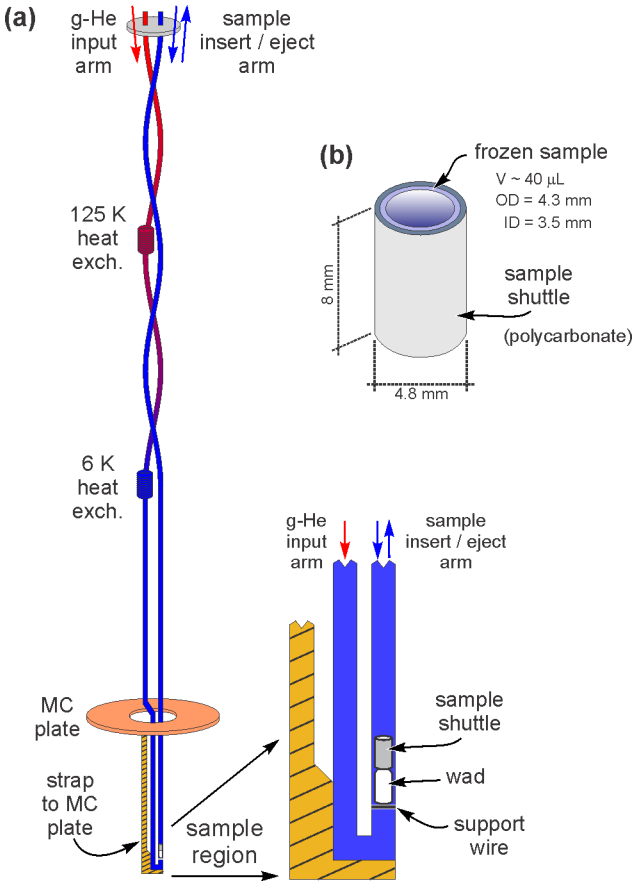

Figure 4. Sample-handling systems. (a) U-tube cryogenic insert. Helical coiling at the top prevents radiative transmission to the bottom, where the sample region is centered in the B field. Sample and wad rest on a support wire (inset). Condensed ^{4}He in the U-tube and an external solid bar couple the sample to cooling power from the mixing chamber (MC) of the DR, and to higher T stages via plates (not shown) between the MC and the 6 K heat exchanger. The 125 K and 6 K exchangers cool gaseous He (99.999%) for pneumatic ejection, as facilitated by a solid Teflon wad behind the open cylindrical sample. (b) Sample geometry and support shuttle.

was dropped in to facilitate eventual pneumatic ejection. Then, a loaded magazine was attached to the I/E arm. Within 20−30 s of exposing this apparatus to room temperature, the frozen sample was released, falling to its rest position (Figure 4a, inset). The I/E arm was then capped, and a volume of ^{4}He was condensed to the U-tube as the sample space cooled to below 4 K. Typically, this was achieved by equilibrating an 11.4 L, room-temperature reservoir containing ∼1/3 atm of 99.999% helium, providing ∼5 mL of liquid He at the base of the U-tube. Although that is less than the 11 mL needed to submerge a sample, contact from either vapor-phase He or a superfluid film was sufficient to thermally sink the sample to cooling from DR components. The latter were coupled to the base of the U-tube by an OFHC rod (Figure 4a) connected to the plate holding the ^{3}He/^{4}He mixing-chamber (MC) of the DR. Both arms of the U-tube are also coupled to higher-temperature DR stages (not shown) via OFHC copper braids. These include plates in the DR for ^{3}He/^{4}He distillation, a 1 K pot, and the previously noted 4 K plate. The latter is also coupled into the bath of liquid He in the cryostat holding the surrounding 14 T magnet.

Sample Ejection and Dissolution. Figure 5a shows the system configured to eject a sample. The path starts near the bottom of the DR cryostat, whose top half appears in the foreground. The I/E arm leads vertically to the top of the DR, where it mates with a vacuum-jacketed bent tube (Figure 5a, top right), in which the indicated low

DOI: 10.1021/jacs.5b01252
J. Am. Chem. Soc. 2015, 137, 8428−8434

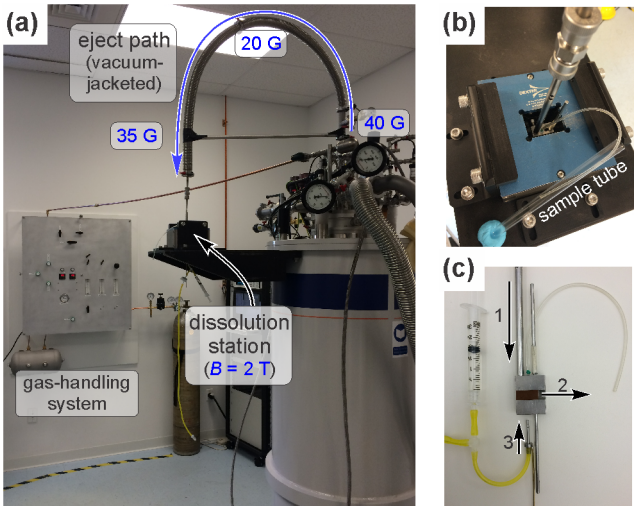

Figure 5. Ejection and dissolution systems. (a) Upper half of DR cryostat in foreground. He flows from the gas-handling system (GHS) to the U-tube described in Figure 4a. A pre-cooled (~80 K) bent tube completes the eject path from the U-tube to a dissolution station at 2 T. The 20–40 G fields on the bent path facilitate LFTM. (b) Dissolution apparatus placed in the ~25 × 15 × 15 mm magnet bore (top view), with adjacent sample tube to receive the solution-state product. (c) Dissolution apparatus (titanium body), in which ejected samples arrive along path 1. Sliding the center piece (Vespel) then moves the sample along path 2, stripping off the wad. Finally, a dissolution pin is inserted along path 3, into the open center of the sample shuttle. Syringe injection of ~2.1 mL of water typically yields a 1 mL solution with near-quantitative transfer.

fields (<50 G) activate LFTM, as described in the Results and Discussion. The bent tube terminates at a dissolution station (detailed below) in the center of a 2 T permanent magnet array (Dexter Magnetics).

Preparation for ejection is initiated before the bent tube is put in place, i.e., when the U-tube is closed with sample at polarizing conditions. To begin, the I/E arm is brought to positive pressure (1 psi) over ~5–10 min, first by boiling off condensed liquid He using a heater on the exterior of the base of the U-tube. That process requires ~5–10 min [$\ll T_1(^1\mathrm{H})$], during which sample T gradually increases to 5 K. Following this, 2.7 L/min is added from the GHS, which is continuously joined to the other arm of the U-tube at the top of the DR cyrostat. That further increases the sample T to ~10 K in ~45 s. Meanwhile, the interior of the bent tube has been pre-cooled to ~80 K using forced liquid N_2. (HP signals were not obtained without this cooling, whereas forced liquid He did not improve results.) When 1 psi relief occurs on the U-tube, 2.7 L/min flow is maintained, and we then connect the pre-cooled bent tube both at the top of the DR and at the dissolution station. Before ejection is actuated, 30–60 s [$\ll T_1(^1\mathrm{H})$] typically goes by with the sample T near 10 K.

Sample ejection was typically driven by a 0.9 s pulse of 120 L/min of He at 3 bar. Time to sample arrival at the dissolution station varied from ~0.4–0.8 s, depending on the path T encountered by the gas. The station sits at 2 T to maintain polarization until the dissolution step. Figure 5b shows the dissolution apparatus inside the 2 T bore, while Figure 5c provides a full view. The caption details the process of sample arrival followed by successive steps for manual actuation of a slider (sample positioner), a dissolution pin, and a syringe of deoxygenated Chromosolv water (Sigma-Aldrich). Those steps typically require ~3 s, triggered by the sound of the sample's arrival. Aqueous output was collected in 10 mm NMR tubes for measurement at 1 T, or occasionally split at a T-junction for simultaneous collection of a second aliquot in a 5 mm tube for high-field, high-resolution NMR. Sample concentrations (typically 200–300 mM) were determined by analysis of integrated signals from high-resolution spectra vs a standard series.

NMR Measurements. High-resolution $^{13}\mathrm{C}$ spectra were collected on a Bruker Avance III 400 MHz spectrometer (100.6 MHz $^{13}\mathrm{C}$ frequency) using a simple $(\pi/2)$-(detect) sequence with 8.3 μs pulse, 1.3 s acquisition, and 24 kHz spectral width. The HP spectrum was manually initiated after loading the sample with the standard I/E mechanism.

Spin–echo results were obtained on a Bruker MiniSpec mq40 1 T spectrometer (10.06 MHz $^{13}\mathrm{C}$). The pulse sequence $(\pi/2)_x-[\tau-(\pi)_y-\tau]_n$ was employed, with τ = 1.5 ms, $t_{\pi/2}$ and t_π = 19.2 and 39.2 μs, and n = 3800. Acquisitions of HP signals were triggered by an optical sensor tripped when a sample tube was pushed into the NMR probe.

Echo trains were detected on resonance with quadrature sampling (120 kHz) of the central 250 μs (30 points) of each echo. Decay profiles (Figure 2a) were computed as

$$S(t_j) = \sum_{k=1}^{30} (a_{j,k}{}^2 + b_{j,k}{}^2)^{1/2} \tag{2}$$

where t_j is the time at the center of the jth echo, consisting of k = 1–30 complex values, $(a + ib)_{j,k}$. We report "magnitude signals" to indicate the absolute signal intensity in an echo train. This is obtained by first computing a weighted average of echoes,

$$\mathrm{echo}_{\mathrm{avg}} = \sum_{j=1}^{3800} ((a_{j,k} + ib_{j,k})\ \mathrm{e}^{-t_j/\tau}) = \{(a_{\mathrm{avg}} + ib_{\mathrm{avg}})_k\} \tag{3}$$

where the exponential constant, τ = 6.5 s, was used as a reasonable match to the natural decay in all experiments. The magnitude signal is then the single value resulting from

$$S_{\mathrm{mag}} = (\sum_{k=1}^{30} (a_{\mathrm{avg}})_k{}^2 + (b_{\mathrm{avg}})_k{}^2)^{1/2} \tag{4}$$

Constant offsets vs receiver gain were accounted using carefully calibrated measurements on the empty spectrometer. An advantage of the magnitude signal vs decay profiles is that even the non-HP reference yields a reproducible value above the noise in a single scan. In contrast, the decay profile is not discernible in the reference without resorting to hours of signal averaging.

After initial HP measurement, samples were capped to limit O_2-induced relaxation. Single-shot references collected immediately following the HP signal did not differ significantly from those collected following hours-long, signal-averaged reference scans. This indicates that apparently larger enhancements from signal-averaged references were not due to chemical change.

■ ASSOCIATED CONTENT

Supporting Information

Description of T profiles during pre-polarization; results of spin-relaxation experiments near Earth's field; and additional discussion of thermal mixing and multi-sample cooling. The Supporting Information is available free of charge on the ACS Publications website at DOI: 10.1021/jacs.5b01252.

■ AUTHOR INFORMATION

Corresponding Authors

*neal@millikelvintech.com
*james.kempf@bruker.com

Notes

The authors declare the following competing financial interest(s): Millikelvin Technologies (MKT) holds U.S. patent no. 8,703,102 on methods for brute-force hyperpolarization. Bruker and MKT have patents pending on sample handling and environmental control for brute-force HP (U.S. 14/161,172, 14/212,695, and 14/486,115).

DOI: 10.1021/jacs.5b01252
J. Am. Chem. Soc. 2015, 137, 8428–8434

■ ACKNOWLEDGMENTS

We thank Werner Maas of Bruker Biospin for enthusiastic support, and Frank DiFillipi, formerly of Bruker, for design input on sample handling. We thank Prof. Vesna Mitrovic and Lu Lu of Brown University for acquiring early T_1 data.

■ REFERENCES

(1) Thorsten, M.; Debelouchina, G. T.; Bajaj, V. S.; Hu, K. N.; Joo, C. G.; Mak-Jurkauskas, M. L.; Sirigiri, J. R.; van der Wel, P. C. A.; Herzfeld, J.; Temkin, R. J.; Griffin, R. G. *J. Chem. Phys.* **2008**, *128*, No. 052211.
(2) Rosay, M.; Tometich, L.; Pawsey, S.; Bader, R.; Schauwecker, R.; Blank, M.; Borchard, P. M.; Cauffman, S. R.; Felch, K. L.; Weber, R. T.; Temkin, R. J.; Griffin, R. G.; Maas, W. *Phys. Chem. Chem. Phys.* **2010**, *12*, 5850.
(3) Ardenkjær-Larsen, J. H.; Fridlund, B.; Gram, A.; Hansson, G.; Hansson, L.; Lerche, M. H.; Servin, R.; Thaning, M.; Golman, K. *Proc. Natl. Acad. Sci. U.S.A.* **2003**, *100*, 10158.
(4) Koers, E.; van der Cruijsen, E. W.; Rosay, M.; Weingarth, M.; Prokofyev, A.; Sauvée, C.; Ouari, O.; van der Zwan, J.; Pongs, O.; Tordo, P.; Maas, W.; Baldus, M. *J. Biomol. NMR* **2014**, *60*, 157.
(5) Lesage, A.; Lelli, M.; Gajan, D.; Caporini, M. A.; Vitzthum, V.; Miéville, P.; Alauzun, J.; Roussey, A.; Thieuleux, C.; Mehdi, A.; Bodenhausen, G.; Coperet, C.; Emsley, L. *J. Am. Chem. Soc.* **2010**, *132*, 15459.
(6) Rossini, A. J.; Widdifield, C. M.; Zagdoun, A.; Lelli, M.; Schwarzwälder, M.; Copéret, C.; Lesage, A.; Emsley, L. *J. Am. Chem. Soc.* **2014**, *136*, 2324.
(7) Bowen, S.; Hilty, C. *Angew. Chem.* **2008**, *120*, 5313.
(8) Hilty, C.; Bowen, S. *Org. Biomol. Chem.* **2010**, *8*, 3361.
(9) Miclet, E.; Abergel, D.; Bornet, A.; Milani, J.; Jannin, S.; Bodenhausen, G. *J. Phys. Chem. Lett.* **2014**, *5*, 3290.
(10) Lee, Y.; Heo, G. S.; Zeng, H.; Wooley, K. L.; Hilty, C. *J. Am. Chem. Soc.* **2013**, *135*, 4636.
(11) Lerche, M. H.; Meier, S.; Jensen, P. R.; Baumann, H.; Petersen, B. O.; Karlsson, M.; Duus, J.Ø.; Ardenkjær-Larsen, J. H. *J. Magn. Reson.* **2010**, *203*, 52.
(12) Lee, Y.; Zeng, H.; Ruedisser, S.; Gossert, A. D.; Hilty, C. *J. Am. Chem. Soc.* **2012**, *134*, 17448.
(13) Lerche, M. H.; Jensen, P. R.; Karlsson, M.; Meier, S. *Anal. Chem.* **2015**, *87*, 119.
(14) Harris, T.; Szekely, O.; Frydman, L. *J. Phys. Chem. B* **2014**, *118*, 3281.
(15) Zeng, H.; Bowen, S.; Hilty, C. *J. Magn. Reson.* **2009**, *199*, 159.
(16) Bowers, C. R.; Weitekamp, D. P. *J. Am. Chem. Soc.* **1987**, *109*, 5541.
(17) Bhattacharya, P.; Harris, K.; Lin, A. P.; Mansson, M.; Norton, V. A.; Perman, W. H.; Weitekamp, D. P.; Ross, B. D. *MAGMA* **2005**, *18*, 245.
(18) Bhattacharya, P.; Chekmenev, E. Y.; Perman, W. H.; Harris, K. C.; Lin, A. P.; Norton, V. A.; Tan, C. T.; Ross, B. D.; Weitekamp, D. P. *J. Magn. Reson.* **2007**, *186*, 150.
(19) Adams, R. W.; Aguilar, J. A.; Atkinson, K. D.; Cowley, M. J.; Elliott, P. I. P.; Duckett, S. B.; Green, G. G. R.; Khazal, I. G.; López-Serrano, J.; Williamson, D. C. *Science* **2009**, *323*, 1708.
(20) Theis, T.; Truong, M.; Coffey, A. M.; Chekmenev, E. Y.; Warren, W. S. *J. Magn. Reson.* **2014**, *248*, 23.
(21) Reineri, F.; Boi, T.; Aime, S. *Nature Commun.* **2015**, *6*, 5858.
(22) Brindle, K. M.; Bohndiek, S. E.; Gallagher, F. A.; Kettunen, M. I. *Magn. Reson. Med.* **2011**, *66*, 505.
(23) Harris, T.; Eliyahu, G.; Frydman, L.; Degani, H. *Proc. Natl. Acad. Sci. U.S.A.* **2009**, *106*, 18131.
(24) Day, S. E.; Kettunen, M. I.; Gallagher, F. A.; Hu, D.-E.; Lerche, M.; Wolber, J.; Golman, K.; Ardenkjaer-Larsen, J. H.; Brindle, K. M. *Nat. Med.* **2007**, *13*, 1382.
(25) Nelson, S. J.; Kurhanewicz, J.; Vigneron, D. B.; Larson, P. E.; Harzstark, A. L.; Ferrone, M.; van Criekinge, M.; Chang, J. W.; Bok, R.; Park, I.; Reed, G.; Carvajal, L.; Small, E. J.; Munster, P.; Weinberg, V. K.; Ardenkjaer-Larsen, J. H.; Chen, A. P.; Hurd, R. E.; Odegardstuen, L. I.; Robb, F. J.; Tropp, J.; Murray, J. A. *Sci. Trans. Med.* **2013**, *5*, No. 198ra108.
(26) Spence, M. M.; Rubin, S. M.; Dimitrov, I. E.; Ruiz, E. J.; Wemmer, D. E.; Pines, A.; Yao, S. Q.; Tian, F.; Schultz, P. G. *Proc. Natl. Acad. Sci. U.S.A.* **2001**, *98*, 10654.
(27) Boutin, C.; Desvaux, H.; Carrière, M.; Leteurtre, F.; Jamin, N.; Boulard, Y.; Berthault, P. *NMR Biomed.* **2011**, *24*, 1264.
(28) Bai, Y.; Hill, P. A.; Dmochowski, I. J. *Anal. Chem.* **2012**, *84*, 9935.
(29) Kuhn, L. T. *Top. Curr. Chem.* **2013**, *338*, 229.
(30) Saha, G. B. *Basics of PET Imaging: Physics, Chemistry and Regulations*; Springer Science & Business Media: New York, 2005.
(31) Dalitz, F.; Cudaj, M.; Maiwald, M.; Guthausen, G. *Prog. NMR Spectrosc.* **2012**, *60*, 52.
(32) Jannin, S.; Bornet, A.; Colombo, S.; Bodenhausen, G. *Chem. Phys. Lett.* **2011**, *517*, 234.
(33) Jannin, S.; Bornet, A.; Melzi, R.; Bodenhausen, G. *Chem. Phys. Lett.* **2012**, *549*, 99.
(34) Milani, J.; Vuichoud, B.; Bornet, A.; Miéville, P.; Mottier, R.; Jannin, S.; Bodenhausen, G. *Rev. Sci. Instrum.* **2015**, *86*, No. 024101.
(35) Miéville, P.; Ahuja, P.; Sarkar, R.; Jannin, S.; Vasos, P. R.; Gerber-Lemaire, S.; Mishkovsky, M.; Comment, A.; Gruetter, R.; Ouari, O.; Tordo, P.; Bodenhausen, G. *Angew. Chem., Int. Ed.* **2010**, *49*, 6182.
(36) Kempf, J. G.; Kalechofsky, N.; Rosay, M. Sample Preparation Method to Manipulate Nuclear Spin-Relaxation Times, Including to Facilitate Ultralow Temperature Hyperpolarization. U.S. Patent Appl. 14/161,172, Jan 22, 2014.
(37) Abragam, A.; Proctor, W. G. *Phys. Rev.* **1957**, *106*, 160.
(38) Abragam, A.; Proctor, W. G. *Phys. Rev.* **1958**, *109*, 1441.
(39) Gadian, D. G.; Panesar, K. S.; Linde, A. J. P.; Horsewill, A. J.; Kockenberger, W.; Owers-Bradley, J. R. *Phys. Chem. Chem. Phys.* **2012**, *14*, 5397.
(40) Cherubini, A.; Payne, G.; Leach, M.; Bifone, A. *Chem. Phys. Lett.* **2003**, *371*, 640.
(41) Lisitza, N.; Muradian, I.; Frederick, E.; Patz, S.; Hatabu, H.; Chekmenev, E. *J. Chem. Phys.* **2009**, *131*, No. 044508.
(42) Peat, D. T.; Horsewill, A. J.; Kockenberger, W.; Linde, A. J. P.; Gadian, D. G.; Owers-Bradley, J. R. *Phys. Chem. Chem. Phys.* **2013**, *15*, 7586.
(43) Owers-Bradley, J. R.; Horsewill, A. J.; Peat, D. T.; Goh, K. S. K.; Gadian, D. G. *Phys. Chem. Chem. Phys.* **2013**, *15*, 10413.
(44) Friedman, L. J.; Millet, P. J.; Richardson, R. C. *Phys. Rev. Lett.* **1981**, *47*, 1078.
(45) Krjukov, E. V.; O'Neill, J. D.; Owers-Bradley, J. R. *J. Low Temp. Phys.* **2005**, *140*, 397.
(46) Köckenberger, W.; Matysik, J. In *Encyclopedia of Spectroscopy and Spectrometry*, 2nd ed.; Lindon, J. C., Ed.; Academic Press: Oxford, 2010; p 963.
(47) *Hyperpolarization Methods in NMR Spectroscopy*; Kuhn, L. T., Ed.; Springer: Berlin, 2013; Vol. *338*.
(48) Mishkovsky, M.; Frydman, L. *Annu. Rev. Phys. Chem.* **2009**, *60*, 429.

DOI: 10.1021/jacs.5b01252
J. Am. Chem. Soc. 2015, 137, 8428−8434